Binding energy of a hydrogenic donor impurity in a rectangular parallelepiped-shaped quantum dot: Quantum confinement and Stark effects

Shu-Shen Li and Jian-Bai Xia

Citation: Journal of Applied Physics **101**, 093716 (2007); doi: 10.1063/1.2734097
View online: http://dx.doi.org/10.1063/1.2734097
View Table of Contents: http://scitation.aip.org/content/aip/journal/jap/101/9?ver=pdfcov
Published by the AIP Publishing

Binding energy of a hydrogenic donor impurity in a rectangular parallelepiped-shaped quantum dot: Quantum confinement and Stark effects

Shu-Shen Li[a] and Jian-Bai Xia
CCAST (World Laboratory), P.O. Box 8730, Beijing 100080 and State Key Laboratory for Superlattices and Microstructures, Institute of Semiconductors, Chinese Academy of Sciences, P.O. Box 912, Beijing 100083, People's Republic of China

(Received 18 January 2007; accepted 19 March 2007; published online 15 May 2007)

We calculate the binding energy of a hydrogenic donor impurity in a rectangular parallelepiped-shaped quantum dot (QD) in the framework of effective-mass envelope-function theory using the plane wave basis. The variation of the binding energy with edge length, position of the impurity, and external electric field is studied in detail. A finite potential model is adopted in our calculations. Compared with the infinite potential model [C. I. Mendoza *et al.*, Phys. Rev. B **71**, 075330 (2005)], the following results are found: (1) if the impurity is located in the interior of the QD, our results give a smaller binding energy than the infinite potential model; (2) the binding energies are more sensitively dependent on the applied electric field in the finite potential model; (3) the infinite potential model cannot give correct results for a small QD edge length for any location of the impurity in the QD; (4) some degeneracy is lifted when the dot is no longer cubic. © *2007 American Institute of Physics*. [DOI: 10.1063/1.2734097]

I. INTRODUCTION

The Stark effect of an impurity state in a quantum dot (QD) is a major subject for QD physics and applications.[1] Kane presented a scheme for implementing a quantum-mechanical computer[2] in which information is encoded into the nuclear spins of donor atoms in doped silicon electronic devices. Logical operations on individual spins are performed using externally applied electric fields, and spin measurements are made using currents of spin-polarized electrons. The realization of such a computer is dependent on future refinements of conventional silicon electronics.

The ground state and the first excited state of an electron in a QD may be employed as a two-level quantum system (qubit). An electromagnetic pulse can be applied to drive an electron from the ground state to the first excited state or to a superposition state of the ground state and the first excited state. To perform a quantum-controlled NOT manipulation, one may simply apply a static electric field by placing a gate near the QD.[3] The same scheme can be implemented using the ground state and the first excited state of an impurity electron in a QD.

The effective-mass envelope-function approximation is suitable for calculating impurity states in nanostructures[4] since it can be carried out on a personal computer and can be widely applied in the design of various photoelectric devices. In the framework of effective-mass envelope-function theory, calculations of electronic states usually adopt the variational method for a hydrogenic donor impurity in QDs.[5–8] Other approaches have been adopted in quantum wells[9] and QDs.[10,11] Juang and Chang showed Stark shifts were enhanced in finite barrier quantum wires.[12] Cruz and Calder investigated theoretically the tunneling effect on the intersubband optical absorption in a quantum well structure subjected to an external electric field perpendicular to the layers.[13] Gangopadhyay and Nag calculated QD energy levels with finite potential barriers in the shape of a cube or a parallelepiped.[14] Califano and Harrison showed that the energy eigenvalues of cubes were equal to those of cuboids of the same volume.[15] A connection rule between the ground state energies was found which allows the calculation of the energy levels of pyramidal QDs using those of cuboids of suitably chosen dimensions, whose solution requires considerably less computational effort.[16] Within a finite potential well model, the impurity binding energy in the absence and in the presence of confined LO-phonon interaction in a cubic QD were calculated by Amrani *et al.* using a variational approach.[17] Assaid *et al.* studied theoretically the quantum size, impurity position, and electric field on the energy of a shallow donor placed anywhere in a GaAs spherical QD in a uniform electric field.[18] The polarizability was estimated by Messaoudi *et al.* for a shallow donor confined to move in a QD with a uniform magnetic field using the Hass variational method in the case of an infinite and a finite barrier potential.[19] It was found that the finite barrier-height effect was important for high fields and large QDs.

Sahoo and Ho presented an accurate numerical calculation for the energy levels and resonance widths of the quasibound states of a confined hydrogen atom in an isolated QD subjected to an external electric field.[20] Resonance positions and widths were reported for a wide range of dot sizes to demonstrate that Stark resonances in a confined hydrogen atom lead to interesting phenomena as a consequence of the quantum confinement of the atom, contrary to the Stark effect on free atoms.

Movilla and Planelles reported numerically calculated

[a]Electronic mail: sslee@red.semi.ac.cn

ground state and binding energies of a hydrogenic donor impurity confined within a spherical QD surrounded by air or a vacuum. Finite spatial steplike potentials allowing the electronic density to partially leak outside the QD were considered.[21]

Friesen developed an effective-mass theory for substitution donors in silicon in an inhomogeneous environment. Valley-orbit coupling was included perturbatively. The Stark effect in Si:P was specifically considered. Unexpectedly, the ground state energy of the donor electron was found to increase with electric field as a consequence of spectral narrowing of the $1s$ manifold.[22]

Recently, Mendoza *et al.*[23] reported a detailed variational calculation of the binding energies of hydrogenic impurities in a cubic QD as a function of both the impurity position and an applied electric field. He found that the binding energy of the impurities is highly dependent on the impurity position, and the electric field splits the energy of the impurities at points in the box which are equivalent in the absence of the electric field. When the impurity is located in the upper half of the cube and the field pushes the particle downward the binding energy decreases, and the Stark shift exhibits a minimum. However, they adopted an infinite potential model in their calculations and only studied the case of equal edge length (cubic QDs).

In this paper, we study the binding energy of a hydrogenic donor impurity in a QD with an applied external electric field in the framework of effective-mass envelope-function theory using the plane wave basis. A finite potential model and different edge lengths of the QD are considered in our calculations.

II. THEORETICAL MODEL

Throughout this paper, the units of length, energy, and external electric field are given in terms of the effective Bohr radius $a^*=\hbar^2\epsilon/m_e^*e^2$, the effective Rydberg constant $R^*=\hbar^2/2m_e^*a^{*2}$, and $F^*=e/2\epsilon a^{*2}$, respectively, where m_e^*, ϵ, and e are the effective mass, dielectric constant, and charge of an electron, respectively.

For a hydrogenic donor impurity located at $\mathbf{r_0}=(x_0,y_0,z_0)$ in a QD with an applied external electric field, the electron envelope-function equation in the framework of the effective-mass approximation is

$$\left[\Delta-\frac{2\alpha}{|\mathbf{r}-\mathbf{r}_0|}+V(\mathbf{r})-\mathbf{F}\cdot\mathbf{r}\right]\psi_n(\mathbf{r})=E_n^\alpha\psi_n(\mathbf{r}), \tag{1}$$

where $\Delta=-\partial^2/\partial x^2-\partial^2/\partial y^2-\partial^2/\partial z^2$, $\mathbf{r}=(x,y,z)$, and $|\mathbf{r}-\mathbf{r_0}|=\sqrt{(x-x_0)^2+(y-y_0)^2+(z-z_0)^2}$. $n=0,1,2,\ldots$ correspond to the ground, first excited, second excited,…, states, respectively. The external electric field $\mathbf{F}$ can be along any direction for different values of θ and ϕ: $\mathbf{F}=(F_x,F_y,F_z)=(F\sin\theta\cos\phi, F\sin\theta\sin\phi, F\cos\theta)$ in the standard spherical coordinate representation. The quantum confining potential energy of an electron in a rectangular parallelepiped-shaped QD is

$$V(\mathbf{r})=\begin{cases}0 & \text{for } |x|\leqslant W_x/2, \quad |y|\leqslant W_y/2 \quad \text{and } |z|\leqslant W_z/2\\ V_0 & \text{for } |x|>W_x/2, \quad \text{or } |y|>W_y/2 \quad \text{or } |z|>W_z/2,\end{cases} \tag{2}$$

where V_0 is the band offset of the electron, and W_x, W_y, and W_z are the edge lengths of the QD along the x, y, and z directions, respectively.

In Eq. (1), α of 0 and 1 correspond to the absence and presence of donors in the nanostructure. The binding energy of the hydrogenic donor impurity ground state is categorically calculated by the following equation:

$$E_b=E_0^0-E_0^1. \tag{3}$$

It should be pointed out that our calculation has been simplified by considering the same effective-mass values in the dot and in the barrier. In fact, the effects on effective-mass mismatches include two aspects. The first is the effect on the electron states. The second is the effect on the impurity states. Our previous calculations indicated that the effective-mass mismatch only affects the high excited states and very weakly affects the ground and low excited states.[3,25,26] The impurity binding energy is weakly affected by the effects on the effective-mass mismatches.[27]

Using the plane wave method, we deploy the electron wave function[24]

$$\psi(x,y,z)=\frac{1}{\sqrt{L_xL_yL_z}}\sum_{n_xn_yn_z}C_{n_xn_yn_z}e^{i[(k_x+n_xK_x)x+(k_y+n_yK_y)y]+(k_z+n_zK_z)z]}, \tag{4}$$

where L_x, L_y, and L_z are the edge lengths of the unit cell along the x, y, and z directions of the coordinate system, respectively. $K_x=2\pi/L_x$, $K_y=2\pi/L_y$, $K_z=2\pi/L_z$, $n_x\in\{-m_x,\ldots,m_x\}$, $n_y\in\{-m_y,\ldots,m_y\}$, and $n_z\in\{-m_z,\ldots,m_z\}$. The plane wave number is $n_{xyz}=n_xn_yn_z=(2m_x+1)(2m_y+1)(2m_z+1)$, where m_x, m_y, m_z are positive integers. We take $L_x=L_y=L_z=L=W_{\max}+2.5a^*$, $K_x=K_y=K_z=K$, and $n_x=n_y=n_z=15$ in the following calculation,[25] where $W_{\max}$ is the maximum edge length of the QD. The previous calculated results indicate that the energy levels almost do not depend on the value of k_x, k_y, and k_z if we take the above edge lengths of the unit cell.[24,25] Therefore, we can simply let $k_x=k_y=k_z=0$ in the following calculations.

The matrix elements for solving the electron energy latent root of the impurity states can be found from Eqs. (1) and (4). The matrix elements contain four parts. The first part includes the matrix elements of the kinetic energy term Δ,

$$[(n_xK)^2+(n_yK)^2+(n_zK)^2]\delta_{n_xn_x'}\delta_{n_yn_y'}\delta_{n_zn_z'}. \tag{5}$$

The second part includes the matrix elements of the donor potential energy term $-2\alpha/|\mathbf{r}-\mathbf{r_0}|$,

$$-\frac{2\alpha}{L^3}\int_{-L/2}^{L/2}dx\int_{-L/2}^{L/2}dy\int_{-L/2}^{L/2}dz$$

$$\times\frac{\exp\{iK[(n_x-n_x')x+(n_y-n_y')y+(n_z-n_z')z]\}}{\sqrt{(x-x_0)^2+(y-y_0)^2+(z-z_0)^2}}. \quad (6)$$

The above integral cannot be evaluated directly. We replace it by $\int_0^{r_0}r^2dr\int_0^{2\pi}d\phi\int_0^{\pi}\sin\theta d\theta$, where $4\pi r_0^3/3=L^3$. When the impurity is not located at the center of the QD, the approximation is somewhat crude. However, the errors are very small for large enough L, as can be checked by comparing our results with that of Ref. 11. Now, the second part of the matrix elements can be approximatively written as

$$-\frac{3\alpha}{r_0}\delta_{n_xn_x'}\delta_{n_yn_y'}\delta_{n_zn_z'}+\frac{6\alpha[\cos(\Lambda r_0)-1]}{r_0^3\Lambda^2}$$

$$\times(1-\delta_{n_xn_x'}\delta_{n_yn_y'}\delta_{n_zn_z'})\exp\{iK[(n_x-n_x')x_0$$

$$+(n_y-n_y')y_0+(n_z-n_z')z_0]\}, \quad (7)$$

with

$$\Lambda=K\sqrt{(n_x-n_x')^2+(n_y-n_y')^2+(n_z-n_z')^2},$$

and

$$\delta_{n_\mu n_\mu'}=\begin{cases}1 & \text{for } n_\mu=n_\mu'\\ 0 & \text{for } n_\mu\neq n_\mu',\end{cases} \quad (8)$$

where μ represents x, y, or z, respectively.

The third part of the matrix elements is deduced from the quantum confined potential $V(\mathbf{r})$,

$$V_0(\delta_{n_xn_x'}\delta_{n_yn_y'}\delta_{n_zn_z'}-S_xS_yS_z), \quad (9)$$

with

$$S_\mu=\begin{cases}W_\mu/L & \text{for } n_\mu=n_\mu'\\ \sin[\pi(n_\mu-n_\mu')W_\mu/L]/\pi(n_\mu-n_\mu') & \text{for } n_\mu\neq n_\mu'.\end{cases} \quad (10)$$

The fourth part of the matrix elements is deduced from the electric field energy $-\mathbf{F}\cdot\mathbf{r}$,

$$-\sum_\mu\langle n_\mu'|\mu F_\mu|n_\mu\rangle, \quad (11)$$

where

$$|n_\mu\rangle=\frac{\exp(i\mu(k_\mu+n_\mu K_\mu))}{\sqrt{L_\mu}}, \quad (12)$$

and

$$\langle n_\mu'|\mu F_\mu|n_\mu'\rangle=\begin{cases}0 & \text{for } n_\mu=n_\mu'\\ \dfrac{iF_\mu(-1)^{(n_\mu-n_\mu')}}{2\pi(n_\mu-n_\mu')} & \text{for } n_\mu\neq n_\mu'.\end{cases} \quad (13)$$

The electronic states in the QD can be calculated from Eqs. (5), (7), (9), and (11).

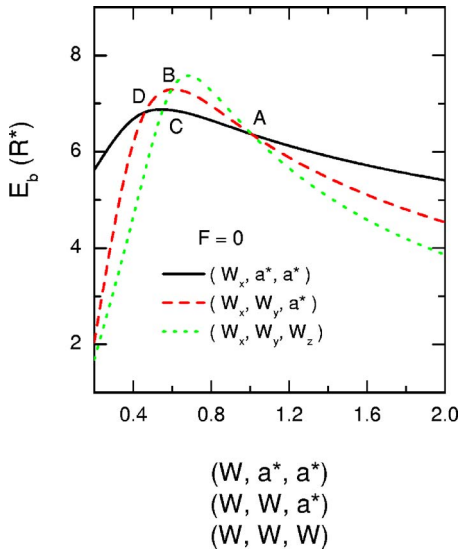

FIG. 1. (Color online) The binding energy of the ground state as a function of the QD edge length W_μ with no external electric field and with the donor located at the QD center. The solid, dashed, and dotted lines correspond to changing W_x while fixing W_y and W_z ($W_y=W_z=a^*$), simultaneously changing W_x and W_y ($W_x=W_y$) while fixing W_z ($W_z=a^*$), and simultaneously changing W_x, W_y, and W_z, respectively.

III. RESULTS AND DISCUSSION

In the following sections we will give some numerical results of the binding energy for a hydrogenic donor impurity in a QD with the conduction-band offset $V_0=40\ R^*$.

Figure 1 shows the binding energy of the ground state as a function of the QD edge length W_μ with no external electric field and with the donor located at the QD center. The solid, dashed, and dotted curves correspond to changing W_x while holding W_y and W_z fixed ($W_y=W_z=a^*$), simultaneously changing W_x and W_y ($W_x=W_y$) while holding W_z fixed ($W_z=a^*$), and simultaneously changing W_x, W_y, and W_z, respectively. From this figure, we find four crossing points A, B, C, and D. Point A corresponds to the impurity binding energy of a cubic QD with edge length $W_x=W_y=W_z=a^*$. Point B corresponds to the edge length W_B for which the impurity has the same binding energy for (W_B,W_B,W_B) and (W_B,W_B,a^*), where (W_x,W_y,W_z) indicates that the edge lengths of the rectangular parallelepiped-shaped QD along the x, y, and z directions are W_x, W_y, and W_z, respectively. Point C corresponds to the edge length W_C for which the impurity has the same binding energy for (W_C,W_C,W_C) and (W_C,a^*,a^*), and point D corresponds to the edge length W_D for which the impurity has the same binding energy for (W_D,W_D,a^*) and (W_D,a^*,a^*). These phenomena show that the binding energy has the same value for two edge length values besides the curve peaks. From this figure we also find that the critical edge lengths corresponding to the maximum binding energy are the smallest, middle, and largest for the solid, dashed, and dotted lines, respectively. In the infinite potential model,[23] the binding energy curves do not exhibit those peaks. Rather, the binding energy becomes infinite as the QD edge length decreases to zero.

The greatest difference between the finite and the infinite potential model is whether the wave function can penetrate

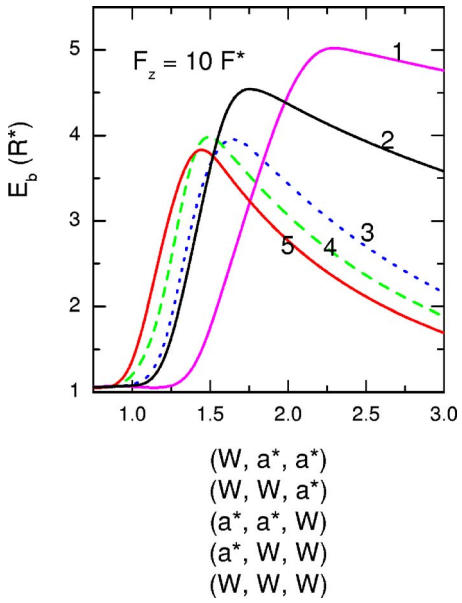

FIG. 2. (Color online) The same as Fig. 1 but with external electric field $F_z=10F^*$ ($\theta=0$) and with the donor located at the center. The curves 1, 2, 3, 4, and 5 correspond to the variation of the binding energy of the ground state with W_x while $W_y=W_z=a^*$, W_x, W_y ($W_x=W_y$) while $W_z=a^*$, W_z while $W_x=W_y=a^*$ (dotted curve), W_y and W_z ($W_y=W_z$) while $W_x=a^*$ (dashed curve), and W_x and W_y and W_z ($W_x=W_y=W_z$), respectively.

into the barrier region. This is the reason that the curves in Fig. 1 have peaks in our results. The three edges of the QD of point A in Fig. 1 are the same length a^*. The lengths of one, two, and three edges are greater than a^* for the curves to the right of point A, so the wave functions are squeezed weakly, strongly, and more strongly and the binding energies slowly, quickly, and more quickly decrease as the transverse coordinates increase for the solid, dashed, and dotted curves, respectively. If the transverse coordinates are smaller than that of point A, then one, two, and three edge lengths decrease as the transverse coordinates decrease, and the wave functions are squeezed along one, two, and three directions, so the binding energies increase slowly, quickly, and more quickly for the solid, dashed, and dotted curves, respectively. However, if the binding energies pass the peaks, the binding energies will slowly, quickly, and more quickly decrease for the solid, dashed, and dotted curves, respectively. This is because the wave functions more intensively penetrate into the barrier along one, two, and three directions for the solid, dashed, and dotted curves, respectively.

Figure 2 is the same as Fig. 1 but with an external electric field $F_z=10F^*$ ($\theta=0$) and with the donor located at the center. The curves 1, 2, 3, 4, and 5 correspond to the binding energy of the ground state when varying W_x while $W_y=W_z=a^*$, when varying W_x and W_y ($W_x=W_y$) while $W_z=a^*$, when varying W_z while $W_x=W_y=a^*$, when varying W_y and W_z ($W_y=W_z$) while $W_x=a^*$ and when varying W_x and W_y and W_z ($W_x=W_y=W_z$), respectively. The external electric field cancels the degeneracy between 1 and 3 (dotted curve), and between 2 and 4 (dashed curve). Compared with Fig. 1, we find that the external electric field moves the peaks toward larger edge lengths while simultaneously lowering the binding energy. The crossing points between the different curves in this figure can be explained similarly as in Fig. 1.

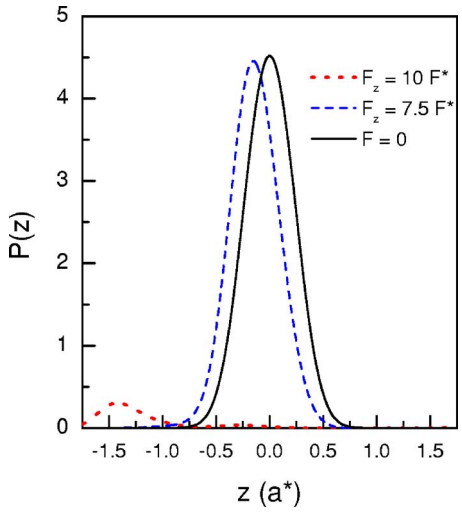

FIG. 3. (Color online) The integrated probability density $P(z)$ with the donor located at the center and $W_x=W_y=W_z=a^*$ for an external electric field $F_z=0$ (solid line), $7.5F^*$ (dashed line), and $10F^*$ (dotted line).

The integrated probability density $P(z)=\int_{-L/2}^{L/2}\int_{-L/2}^{L/2}|\psi_0(x,y,z)|^2dxdy$ is drawn in Fig. 3 with the donor located at the center and $W_x=W_y=W_z=a^*$ for applied external electric fields $F_z=0$ (solid line), $7.5F^*$ (dashed line), and $10F^*$ (dotted line). This figure indicates that the ground state wave function can clearly penetrate the barrier if the electric field is greater than the critical value of $7.5F^*$. If the electric field is smaller than $10F^*$, the ground state wave function does not clearly stride over the side of the supercell. So, our model is effective if the applied external electric field is smaller than $10F^*$.

Figure 4 illustrates the binding energy of the ground state as a function of the magnitude of an electric field in the z direction with the impurity located at various positions in a cubic QD (points a, b, b', b'', c, c', and d) which are shown in the inset of the figure. The edge length is taken as $W_x=W_y=W_z=a^*$ (for GaAs a^* is about 10 nm). The dotted

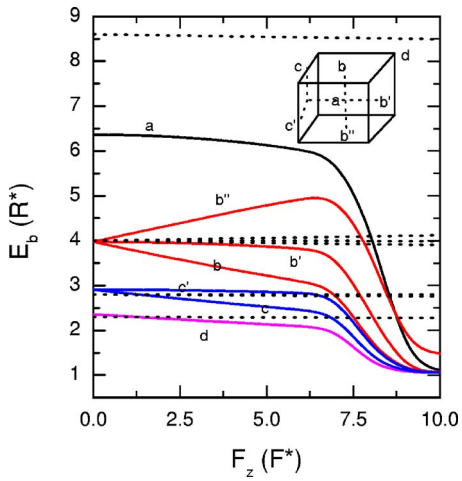

FIG. 4. (Color online) The binding energy in positions a, b, c, and d as a function of the magnitude of the electric field in the z direction, for $W_x=W_y=W_z=a^*$. The dotted curves are the results of Ref. 23.

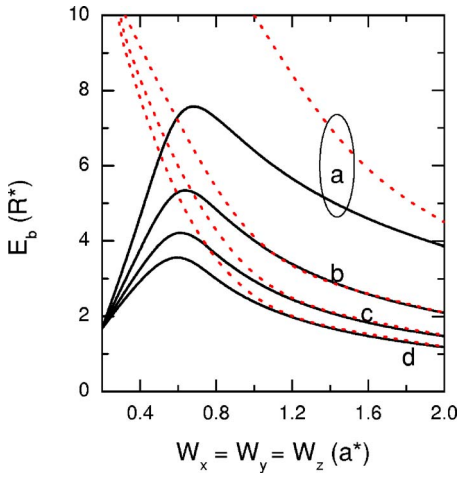

FIG. 5. (Color online) The binding energy in positions a, b, c, and d as a function of cubic QD edge length ($W_x=W_y=W_z$) for zero external electric field. The dotted curves are the results of Ref. 23.

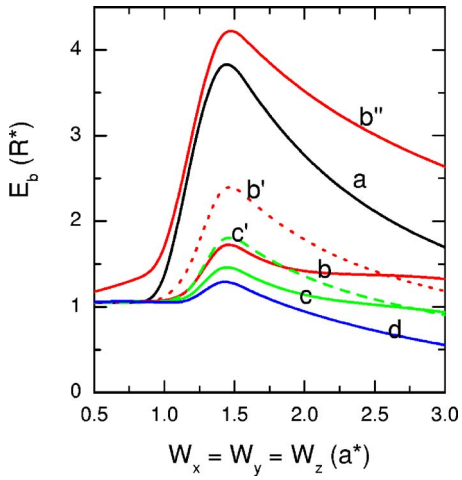

FIG. 6. (Color online) The same as Fig. 4, but with $F=F_z=10F^*$, and including additional points b' (dotted curves), b'', and c' (dashed curve).

curves are the results of Mendoza *et al.* with the infinite potential model.[23] Comparing our results with those of Mendoza, the following differences can be found: (a) if the impurity is located in the interior of the QD (for example, at the center, curve a), our finite potential model gives a smaller binding energy than that of the infinite potential model for any electric field; (b) if the impurity is located exactly on the QD border, the two models give very close binding energies for zero electric field; (c) the binding energies are more sensitively dependent on the applied electric field in our finite potential model; (d) when the electric field is greater than about $7.5F^*$, the binding energies quickly decrease to $1R^*$ except when the impurity is located at point b''. This is because the electric field pushes the impurity wave function into the barrier material. When the electric field is greater than about $7.5F^*$, almost the whole wave function is located in the barrier material, so the binding energy is close to the binding energy of bulk material ($1R^*$). However, the electric field pushes point b'' impurity wave function into the interior of the QD, resulting in a binding energy somewhat greater than R^*.

Figure 5 indicates the binding energy for positions a, b, c, and d as a function of the cubic QD edge length ($W_x=W_y=W_z$) for zero external electric field. The dotted curves are the results of Mendoza *et al.*[23] From this figure we find that (a) the infinite potential model cannot give the correct results for a small QD edge length for any location of the impurity in the QD; (b) for any finite edge length, the binding energies gotten from the infinite potential model are greater than the results of our finite potential model if the impurity is located at the QD center; (c) if the QD edge length is greater than a^*, the two models give very close binding energies when the impurity is located at one of the QD sides.

Figure 6 is the same as Fig. 4, but with $F=F_z=10\ F^*$. The binding energy degeneracy between positions b, b', and b'' and between c and c' is canceled by the applied external electric field. Compared with the results of the infinite potential model (Fig. 6 of Ref. 23), two differences can be found besides those appearing in Fig. 6. First, the binding energy of b'' is always greater than that of the center position a in our finite potential model. But for the infinite potential model, the binding energy of a is greater than that of b'' for small QD edge lengths. Secondly, the crossing points that are found between the binding energies of b and b' (dotted curve) and between c and c' (dashed curve) in our results do not appear in the infinite potential model.[23]

The method presented in this paper can be easily used to calculate how the impurity states change with the direction of an external electric field. Figure 7 shows the impurity binding energy as a function of the external electric field for a cubic QD with edge length a^* with an impurity located at the center of the QD. The solid and dotted curves indicate the results for an electric field along the diagonal ($\theta=\phi=\pi/4$) and z directions ($\theta=0$). From this figure, we find that if the external electric field is greater than $5F^*$, the binding energy sensitively depends on the electric field direction. For QDs of other shapes (with lower symmetry than a cubic QD), the impurity states will be more sensitively dependent on the external electric field.[26]

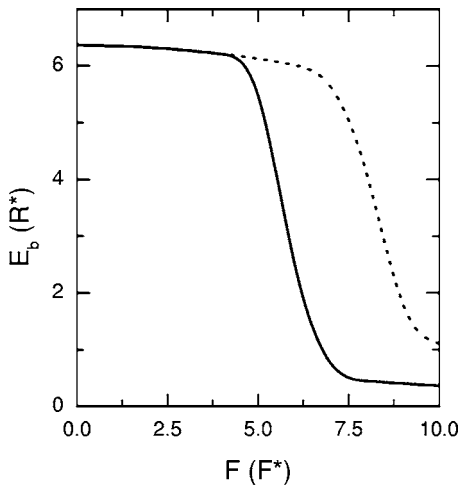

FIG. 7. The impurity binding energy as a function of external electric field for the a^* edge length and the impurity located at the center of the cubic QD. The solid and dotted curves indicate the results for an electric field along the diagonal ($\theta=\phi=\pi/4$) and z directions ($\theta=0$).

TABLE I. The binding energies of the six symmetry points. The coordinates and energy are in units of R^* and a^*. The edge lengths of the QD are $W_x=0.5a^*$, $W_y=1a^*$, and $W_x=1.5a^*$.

Coordinates	(0.25, 0, 0)	(−0.25, 0, 0)	(0, 0.5, 0)	(0, 0.5, 0)	(0, 0, 0.75)	(0, 0, −0.75)
E_b for $F=0$	5.06	5.06	3.93	3.93	3.28	3.28
E_b for $F_z=10F^*$	4.54	4.54	3.58	3.58	2.09	4.76

Some degeneracy is lifted when the dot is no longer cubic. Table I shows the binding energies of the ground state for the six symmetry points located at the centers of the six QD faces. The edge lengths of the QD are $W_x=0.5a^*$, $W_y=1a^*$, and $W_x=1.5a^*$. The coordinate values of the six points are indicated in the brackets. For the cubic QD, the binding energies of the six symmetry points are equal. For a rectangular parallelepiped-shaped QD, however, the binding energies are only equal for the face-to-face points. The binding energies' degeneracy will be lifted for the two face-to-face points along the z direction if a static electric field is applied along that direction.

It must be pointed out that the application of the electric field can also produce quasibound states.[13,20] We will continue to research this topic in our following work.

IV. CONCLUSION

In summary, we have calculated the binding energy of a hydrogenic donor impurity in a rectangular parallelepiped-shaped QD in the framework of effective-mass envelope-function theory using the plane wave basis. The finite potential model was adopted in our calculation. Compared with the previous infinite potential model, some results were found. The calculation method presented in this paper can be easily used to calculate how the impurity states change with the direction of the external electric field. Our calculated results are useful for the application of QDs in photoelectric and electronic devices.

ACKNOWLEDGMENT

This work was supported by the National Natural Science Foundation Nos. 90301007, 60521001, 60328407, 60325416 of China.

[1] A. D. Yoffe, Adv. Phys. **51**, 1 (2001).
[2] B. E. Kane, Nature (London) **393**, 133 (1998).
[3] S.-S. Li, J.-B. Xia, J.-L. Liu, F.-H. Yang, Z.-C. Niu, S.-L. Feng, and H.-Z. Zheng, J. Appl. Phys. **90**, 6151 (2001).
[4] S. B. Orlinskii, J. Schmidt, E. J. J. Groenen, P. G. Baranov, C. de Mello Donegá, and A. Meijerink, Phys. Rev. Lett. **94**, 097602 (2005).
[5] N. Porras-Montenegro and S. T. Perez-Merchancano, Phys. Rev. B **46**, 9780 (1992).
[6] N. Porras-Montenegro, S. T. Perez-Merchancano, and A. Latge, J. Appl. Phys. **74**, 7624 (1993).
[7] C. Bose, J. Appl. Phys. **83**, 3089 (1998).
[8] C. Bose and K. Sarkarc, Physica B **253**, 238 (1998).
[9] Z. P. Liu and T. K. Li, J. Phys. C **18**, 691 (1985).
[10] J. L. Zhu, J. H. Zhao, and J. J. Xiong, Phys. Rev. B **50**, 1832 (1994).
[11] J. L. Zhu and X. Chen, Phys. Rev. B **50**, 4497 (1994).
[12] C. Juang and C. Y. Chang, Appl. Phys. Lett. **58**, 1527 (1991).
[13] G. González de la Cruz and A. Calderón, Solid State Commun. **98**, 553 (1996).
[14] S. Gangopadhyay and B. R. Nag, Nanotechnology **8**, 14 (1997).
[15] M. Califano and P. Harrison, J. Appl. Phys. **86**, 5054 (1999).
[16] M. Califano and P. Harrison, J. Appl. Phys. **88**, 5870 (2000).
[17] B. El Amrani, M. Barnoussi, M. Fliyou, M. Chaouch, and S. Sayouri, Phys. Status Solidi B **226**, 393 (2001).
[18] E. Assaid, E. Feddi, M. Khaidar, F. Dujardin, and B. Stébé, Phys. Scr. **63**, 329 (2001).
[19] K. El Messaoudi, A. Zounoubi, I. Zorkani, and A. Jorio, Phys. Status Solidi B **233**, 270 (2002).
[20] S. Sahoo and Y. K. Ho, Phys. Rev. B **bf69**, 165323 (2004).
[21] J. L. Movilla and J. Planelles, Phys. Rev. B **71**, 075319 (2005).
[22] M. Friesen, Phys. Rev. Lett. **94**, 186403 (2005).
[23] C. I. Mendoza, G. J. Vazquez, M. del Castillo-Mussot, and H. Spector, Phys. Rev. B **71**, 075330 (2005).
[24] M. A. Cusack, P. R. Briddon, and M. Jaros, Phys. Rev. B **54**, R2300 (1996).
[25] S.-S. Li and J.-B. Xia, Chin. Phys. Lett. **23**, 1896 (2006).
[26] S.-S. Li and J.-B. Xia, Appl. Phys. Lett. **87**, 043102 (2005).
[27] S.-S. Li and X.-J. Kong, J. Phys.: Condens. Matter **4**, 4815 (1992).